To appear in the Astrophysical Journal

Chandra Detects the Rare Oxygen-type Wolf-Rayet Star WR 142 and OB Stars in Berkeley 87

Kimberly R. Sokal[1], Stephen L. Skinner[1], Svetozar A. Zhekov[2,3], Manuel Güdel[4], and Werner Schmutz[5]

ABSTRACT

We present first results of a *Chandra* X-ray observation of the rare oxygen-type Wolf-Rayet star WR 142 (= Sand 5 = St 3) harbored in the young, heavily-obscured cluster Berkeley 87. Oxygen type WO stars are thought to be the most evolved of the WRs and progenitors of supernovae or gamma ray bursts. As part of an X-ray survey of supposedly single Wolf-Rayet stars, we observed WR 142 and the surrounding Berkeley 87 region with *Chandra* ACIS-I. We detect WR 142 as a faint, yet extremely hard X-ray source. Due to weak emission, its nature as a thermal or nonthermal emitter is unclear and thus we discuss several emission mechanisms. Additionally, we report seven detections and eight non-detections by *Chandra* of massive OB stars in Berkeley 87, two of which are bright yet soft X-ray sources whose spectra provide a dramatic contrast to the hard emission from WR 142.

Subject headings: stars: individual (WR 16, WR 142 = Sand 5 = St 3, BD+36 4032, HD 229059, V439 Cyg) — stars: Wolf-Rayet — open clusters and associations: individual (Berkeley 87) — X-rays: stars

[1]CASA, Univ. of Colorado, Boulder, CO, USA 80309-0389; kimberly.sokal@colorado.edu, stephen.skinner@colorado.edu

[2]JILA, Univ. of Colorado, Boulder, CO, USA 80309-0440

[3]On leave from Space Research Institute, Sofia, Bulgaria

[4]Dept. of Astronomy, Univ. of Vienna, Türkenschanzstr. 17, A-1180 Vienna, Austria

[5]Physikalisch-Meteorologisches Observatorium Davos and World Radiation Center (PMOD/WRC), Dorfstrasse 33, CH-7260 Davos Dorf, Switzerland

1. Introduction

Wolf-Rayet (WR) stars are massive, highly-evolved stars nearing the end of their lives as supernovae (SN) or as collapsing objects emitting gamma-ray bursts (GRB, e.g. MacFadyen & Woosley 1999, Postnov & Cherepashchuk 2001, Georgy et al. 2009). WR stars undergo rapid mass loss through strong winds, with initial masses of $\geq$25M$\odot$ (Crowther 2007). The classification of WR stars is determined spectroscopically in the optical and is divided among the nitrogen-rich WNs, carbon-rich WCs, and oxygen-rich WOs. For the most part, single WR stars are thought to follow the evolutionary path: O $\rightarrow$ (LBV/RSG) $\rightarrow$ WN $\rightarrow$ WC $\rightarrow$ WO $\rightarrow$ SN [or GRB] (Conti et al. 1983, Crowther 2007). The initial mass of the O star determines whether it passes through an intermediate luminous blue variable (LBV) or red supergiant (RSG) phase (Crowther 2007).

Sanduleak (1971) noticed a class of stars that did not have planetary nebulae (PN) but displayed a WR-like spectrum with strong O VI doublet emission similar to those found in the central stars of PN named the O VI sequence by Smith and Aller (1969). These stars were suggested to be a separate WO sequence of Wolf-Rayet stars (rather than an extension of the WC sequence) by Barlow & Hummer (1982). WO stars are thought to be in the late helium-burning stage, or possibly the carbon-burning stage, where the enhanced oxygen abundance compared to less evolved WR stars is revealed by mass loss stripping (Barlow & Hummer 1982). Of the 298 galactic WR stars in the appended VIIth catalogue of galactic Wolf-Rayet stars (van der Hucht 2001, 2006), only four are of the rare WO spectral type, including the star WR 142, also known as Sand 5 (Sanduleak 1971) and St 3 (Stephenson 1966). Crowther et al. (1998) developed a new classification scheme using primary and secondary oxygen line ratios that confirmed previous classifications of WR 142 as a member of the subclass WO2 (Barlow & Hummer 1982, Kingsburgh et al. 1995).

Despite new discoveries of WR stars in the galactic plane, including a WO type as the exciting star of the planetary nebula Th 2-A (Weidmann et al. 2008), little is yet understood about the mechanisms that drive high-energy processes such as X-ray emission in single WR stars, particularly so for the rare WO stars. Although WR stars have much stronger winds and are more evolved chemically, the line-driven instabilities that are thought to give rise to soft X-rays (kT $<$ 1 keV) from shocks in O star winds may also be present in WR winds (Gayley & Owocki 1995). If that is the case, then WR stars may also be capable of producing soft X-rays from radiative wind shocks (Baum et al. 1992).

Few single WR stars had been studied with high sensitivity in X-rays until recently. Thus far, several apparently single WN stars have been observed to emit X-rays (Skinner et al. 2002, Ignace et al. 2003, Oskinova 2005). An ongoing *Chandra* and *XMM-Newton* survey has recently detected the apparently single WN stars WR 2, WR 18, WR 79a, and WR 134

with X-ray luminosities log $L_X \approx 32.2$ - 32.7 erg s^{-1} (Skinner et al. 2010b), comparable to some WR+OB binaries like γ^2 Vel (WC8+O7) with log $L_X = 32.9$ erg s^{-1} (Skinner et al. 2001) or WR 147 (WN8+OB) with log $L_X = 32.83$ erg s^{-1} (Skinner et al. 2007; see also Sec. 4.4). Only upper limits of log $L_X < 29.82$ - 30.97 erg s^{-1} exist from observations of single WC stars (Oskinova et al. 2003, Skinner et al. 2006). The WC sequence is thus either faint in the X-rays or possibly X-ray quiet. WR 142 just recently became the first WO star to be detected in the X-rays using *XMM-Newton* (Oskinova et al. 2009).

WR 142 resides in the open cluster Berkeley 87. Table 1 summarizes the general properties of WR 142. Berkeley 87 lies in a heavily obscured region of the Milky Way in Cygnus. Initial cluster age estimates of $\sim$ 1 - 2 Myr (Turner & Forbes 1982, hereafter TF82) have now been revised upward. A study restricted to three of the highest mass cluster stars suggests a slightly older age of $\sim$ 3 Myr (Massey et al. 2001). A more recent study (Turner et al. 2010) gives $\sim$ 5 Myr. Berkeley 87 is an interesting cluster containing $\approx$ 105 cluster members identified by an optical study (TF82), B-supergiants including HD 229059, an O8.5-O9 star BD+36 4032, a possible luminous blue variable Be star V439 Cyg, and the pulsating M3-supergiant BC Cyg. Additionally, OH masers and compact HII regions trace massive star formation $3'$ - $9'$ north of WR 142 (Argon et al. 2000, Matthews et al. 1973). At a distance of 1230 $\pm$ 40 pc (Turner et al. 2006), the proximity of Berkeley 87 offers ample opportunity to learn about the properties of rare objects such as WR 142 as well as the surrounding cluster.

As part of an X-ray survey aimed at determining if single Wolf-Rayet stars that are not known to be in binary systems are X-ray emitters (specifically which spectral types), we observed WR 142 with *Chandra*. We are unaware of any evidence pointing to a companion of WR 142. WR 142 was chosen over other WO stars because of its relatively nearby distance, low A_V compared to other WR stars, and interesting surrounding cluster. Its astonishing supersonic wind ($v_\infty = 5500$ km s^{-1}, Kingsburgh et al. 1995) and an unusual optical detection of diffuse emission from the C IV doublet (Polcaro et al. 1991) that is a signature of shocked gas make WR 142 an even more interesting target as one of the few oxygen-type WR stars.

The primary objective of the study presented here is to determine the X-ray properties of WR 142. X-ray emission from WR 142 was previously observed by *XMM-Newton* (Oskinova et al. 2009), but *Chandra* has several advantages over *XMM-Newton*, including improved angular resolution (by a factor of $\sim$ 4 - 5), sharp on-axis point-spread function (PSF) to provide checks on source extent, longer uninterrupted exposure that provides a continuous light curve and more stringent test for variability, and lower instrumental background. Such benefits allow for reliable source identification, especially when compared with optical positions; negligible background subtraction for lightcurves and spectra; and searches for the

presence of diffuse shock emission around WR 142. We analyze the faint X-ray spectrum of WR 142 and discuss possible X-ray emission mechanisms. We also report *Chandra* detections of seven other massive OB stars in Berkeley 87 and compare the much softer spectra from two X-ray bright OB stars to the hard spectrum of WR 142. In this paper, we focus on WR 142 and massive OB stars in Berkeley 87. A first overview of the *Chandra* results for the cluster as a whole was presented by Skinner et al. (2010a) and the cluster will be discussed in more detail in a future paper.

2. Chandra Observations and Data Reduction

The *Chandra* observation (ObsID 9914) centered near WR 142 began on 2009 February 2 at 02:41:24 TT and ended on February 2 at 22:52:55 TT. The nominal pointing coordinates were located 28″ NE of WR 142 at R.A. = $20h\,21m\,46.42s$, Decl. = $+37^\circ\,22'\,44.9''$ (J2000.0). The observation was obtained with the ACIS-I (Advanced CCD Imaging Spectrometer) imaging array in faint timed-event mode with 3.2 s frame times. The exposure live time was 70148 s. ACIS-I consists of four front-illuminated 1024 × 1024 pixel CCDs with pixel size $\approx 0.492''$ and has a combined field of view (FOV) of $\approx 16.9' \times 16.9'$. More information on *Chandra* and its instrumentation can be found in the *Chandra* Proposer's Observatory Guide (POG)[6].

The *Chandra* X-ray Center (CXC) provided a Level 2 events file, which was analyzed with CIAO version 4.1.2[7] using standard science threads. To determine the source centroid position, the net counts, and a 3σ extraction region of the target WR 142, we used the CIAO *wavdetect* tool. We ran *wavdetect* on full-resolution images using events in the 0.3 - 8 keV range, chosen to reduce background. The *wavdetect* threshold was set at $sigthresh = 1 \times 10^{-6}$. Scale sizes of 1, 2, 4, 8, and 16 were used. The 3σ extraction region determined for WR 142 by *wavdetect* was an ellipse with an area of ≈ 11.25 pixels^2 (Figure 1) and was used for spectral and timing analysis. The CIAO task *srcextent*, which utilized point-spread-function (PSF) information, was also used to determine the source size of WR 142 and determine if its emission is point-like or extended.

Within the 0.3 - 8 keV energy range, light curves were extracted using CIAO *dmextract* and source variability was tested by two different methods. Using unbinned photon arrival times, we applied the Kolmogorov-Smirnov (KS) test (Press et al. 1992). For comparison,

[6]See http://asc.harvard.edu/proposer/POG

[7]Further information on *Chandra* Interactive Analysis of Observations (CIAO) software can be found at http://asc.harvard.edu/ciao.

the Gregory-Loredo algorithm (Gregory & Loredo 1992, 1996) was applied by using CIAO *glvary*[8] tool.

CIAO *specextract* was used to extract source and background spectra. The tool *specextract* also created response matrix files (RMFs) and auxiliary response files (ARFs). Spectral analysis utilized the HEASOFT *Xanadu*[9] software package including XSPEC vers. 12.5.0. The background region was chosen to be a source-free annulus centered on WR 142 of r = 4 to r = 16 pixels. From this region, we estimate < 1 background count (0.3 - 8 keV) inside the 3σ elliptical source region for WR 142. The background inside the source region is negligible relative to the number of source counts.

3. Results

3.1. Imaging and Source Identification

WR 142 is detected by *Chandra* as an X-ray source at J202144.35+372230.7 (Figure 1). Table 2 summarizes some properties of the X-ray emission from WR 142. These coordinates are the source centroid as determined by *wavdetect* using an energy filtered image (0.3 - 8 keV). Without further astrometric calibration, the *Chandra* ACIS-I absolute position has an accuracy of $\approx 0.4''$ (68% limit)[10]. The X-ray position of WR 142 is in exact agreement with the 2MASS position of J202144.35+372230.7. Additionally, the *Chandra* position has offsets from optical counterparts of only $0.20''$ from the USNO-B1.0 source at J202144.35+372230.9 and $0.23''$ from the HST GSC2.3.2 source at J202144.36+372230.5. All offsets are well within the positional accuracy of *Chandra*.

Results from the CIAO tool *srcextent* indicate WR 142 is not extended. Use of a PSF file specifically tailored for our observation with the WR 142 spectrum and the position of WR 142 on the ACIS-I detector yields a source size of only $0.52''$ (0.41-$0.64''$, 90% confidence), equivalent to about one ACIS pixel, and a PSF size of $0.85''$ (0.66-$1.03''$, 90% confidence). Thus, the X-ray emission of WR 142 is not extended at the 90% confidence level.

---

[8]http://cxc.harvard.edu/ciao/ahelp/glvary.html.

[9]The XANADU X-ray analysis software package is developed and maintained by NASA's High Energy Astrophysics Science Archive Research Center (HEASARC). See http://heasarc.gsfc.nasa.gov/docs/xanadu/xanadu.html for further information.

[10]http://cxc.harvard.edu/cal/ASPECT/celmon/.

3.2. Spectral Analysis

The X-rays from WR 142 are weak but extremely hard, with a mean photon energy of 4.31 keV (Table 2). Surprisingly, WR 142 does not exhibit any significant emission below 2 keV and there is no evidence of a soft component (Figures 2, 3). We find only one event below 2 keV, with an energy of 1.89 keV. This is in contrast to a faint soft component at E $\leq$ 1 keV in the *XMM-Newton* EPIC MOS spectrum of WR 142 reported by Oskinova et al. (2009). Assuming that no variability occurred in the WR 142 source spectrum or N_H between the two observations, the most likely explanation for this difference would be the much lower effective area of *Chandra* ACIS-I at low energies E $\leq$ 1 keV.

We tried to fit the spectrum of WR 142 (Figure 3) with several different models: a 1T (one temperature) APEC optically thin plasma model and a power-law model. The APEC model requires a very high temperature and thus a thermal bremsstrahlung model is similar. Because of low counts, the spectral fit results were somewhat sensitive to binning strategy. Representative spectral fits are shown in Table 3, based on fits of unbinned spectra. Between the different models, there is little variation in the quality of fit using C-statistics (Cash 1979). However, determining whether a particular model is statistically acceptable using C-statistics is not as straightforward as with χ^2 statistics (Heinrich 2003).

Allowing the abundances to vary from solar displays no significant improvement to the APEC fits, nor does the use of representative WO abundances (Table 3). This is largely because we do not detect any emission lines in the spectrum from elements such as O which are highly nonsolar in WO stars. Additionally, all of the O and C lines that lie in the *Chandra* bandpass are below 1 keV where we do not detect any signal.

The data show a slight preference for a model that includes a gaussian line for an iron line in the $\approx$ 6.4 - 6.67 keV energy range (Table 3). The counts from WR 142 are not sufficient to distinguish between the possible iron lines. The event energies closest to the possible iron emission, 6.24, 6.40, 6.60, and 6.63 keV, show two events within 0.1 keV of the iron K line complex at 6.67 keV (Fe XXV He-like triplet). If a weak Fe line is present, it is likely to be the 6.67 keV iron K line, which has been detected in other WR stars.

We have also experimented with fits of binned spectra using χ^2 statistics in order to estimate confidence bounds on important fit parameters (F_X, N_H, kT, Γ_{pow}). Given the limited number of counts (46), binning at desired levels of >10 counts per bin for fitting with χ^2 statistics was not feasible. We thus consider spectra binned to a minimum of 6 counts per bin. Results indicate that if the plasma is thermal, as the APEC models assume, then the temperature kT must be very high, with a lower 90% confidence bound of kT > 3.6 keV (Table 3). The *Chandra* data do not place a useful upper bound on kT.

In determining the X-ray flux, the unbinned spectral fits display fairly consistent results. The fit with the lowest C-statistic shown in Table 3 gives an observed (absorbed) X-ray flux of $F_X = 1.8$ (0.8 - 2.5) $\times 10^{-14}$ erg s^{-1} cm^{-2} (0.3 - 8 keV, 1σ confidence intervals). The error bounds reflect the range of fluxes measured for the different models in Table 3. The best fit models give X-ray luminosities of log $L_X = 30.72$ - 30.82 (ergs s^{-1}), which are derived from unabsorbed fluxes (0.3 - 8 keV) resulting from different unbinned spectral fits in Table 3.

All indications are that the absorption towards WR 142 is high, with N_H around 4 - 5 $\times 10^{22}$ cm^{-2}. This is about 3 - 4 times higher than the absorption estimated from the observed optical extinction of 1.3×10^{22} cm^{-2} obtained using $A_V \approx 6.1$ (van der Hucht 2001, Gorenstein 1975 conversion). Spectral fits of WR 142 with N_H fixed at the value determined from optical extinction give much larger fit residuals than the fits with larger absorption given in Table 3.

3.3. Timing and Variability Analysis

The source shows no obvious large-scale variations nor flares in its X-ray lightcurve (Figure 4). As for short term variability, KS statistics and the Gregory-Loredo algorithm give a probability of constant count rate of 0.77 and 0.40, respectively. Thus, neither test implies variability at high confidence levels (>90%) on timescales of hours during the <1 day *Chandra* observation.

For purposes of comparing the observed X-ray flux by *Chandra* and the previously published *XMM-Newton* X-ray flux of $F_X = 4 \pm 2 \times 10^{-14}$ erg cm^{-2} s^{-1} from 0.25 - 12 keV (Oskinova et al. 2009), we measure $F_X = 3 \pm 1 \times 10^{-14}$ erg cm^{-2} s^{-1} (0.25 - 12 keV) using an average value of the fluxes from the extended energy range from the three models shown in Table 3. Thus, *Chandra* and *XMM-Newton* X-ray fluxes agree to within the uncertainties. Based on the above flux comparison, any variability over the approximate one year interval between the *Chandra* and *XMM-Newton* observations was a factor of ~ 2 or less.

3.4. Summary of WR 142 X-ray Properties

Based on the *Chandra* data discussed above, the X-ray properties of WR 142 can be summarized as follows: (i) source structure is consistent with a point source at *Chandra*'s angular resolution, (ii) no significant variability is detected over a timescale of ≈ 1 day, (iii) strong X-ray absorption below 2 keV, with an absorption column density (N_H) that is a factor of ≈ 3 - 4 greater than expected from published optical estimates, (iv) no evidence

for a soft X-ray component below 2 keV, (v) a spectrum dominated by hard X-rays above 2 keV that can be fit equally well using a very high temperature thermal plasma model or a power-law model, and (vi) a relatively low X-ray luminosity log L_X(0.3 - 8 keV) = 30.7 - 30.8 ergs s^{-1} (at d = 1.23 kpc), which is $\approx$ 10 times less than found for two X-ray bright OB stars in Berkeley 87 (Section 4). We discuss these properties in more detail below.

4. OB Stars in Berkeley 87

In this section, we comment briefly on OB stars in Berkeley 87 contained in the *Chandra* FOV. We report *Chandra* detections of seven OB stars and identify eight undetected B-type stars (Table 2) that are likely cluster members (TF82). Figure 1 shows the relative positions of the X-ray bright stars and the noteworthy non-detection of the LBV candidate V439 Cyg.

4.1. BD+36 4032

This star was classified as O9V by TF82 (Berkeley 87-25) and was the only object explicitly identified as an O-type star in their catalog of 105 likely members of Berkeley 87. The spectral type was later refined to O8.5 III by Massey et al. (2001), who also estimated the mass to be $M_* = 39\ M_\odot$. BD+36 4032 lies $\approx 3'$ northwest of WR 142.

X-ray characteristics are listed in Table 2. The X-ray spectrum is soft (Figure 3) with almost all of the emission emerging below 2 keV, which is dramatically different than the hard emission from WR 142. Reasonably good fits can be obtained using a solar abundance 1T APEC model with a cool plasma component at kT $\approx$ 0.6 keV (Table 4). The 1T APEC fit can be improved slightly by adding a second temperature component between 1 - 2 keV, but almost all of the emission measure still resides in the cool component.

The best-fit N_H given in Table 4 equates to A_V = 5.1 [4.4 - 6.5] mag (Gorenstein 1975). This is in good agreement with the optically-determined value A_V = 4.8 mag using E(B − V) = 1.60 and A_V = 3E(B − V) (TF82). Thus, the excess X-ray absorption detected in WR 142 is not present toward this O star.

4.2. HD 229059

This B supergiant has V = 8.71 mag and was the brightest member of Berkeley 87 listed by TF82 (Berkeley 87-3). They assigned a spectral type B2 Iabe but Massey et al. (2001)

classified it as B1 Ia.

The *Chandra* spectrum of HD 229059 is nearly identical to that of BD+36 4032 (Figure 3). One noticeable difference is that HD 229059 shows stronger emission in the 1.8 - 1.9 keV range, which is likely due to stronger line emission from the Si XIII triplet (1.84 - 1.87 keV).

Spectral fits of HD 229059 give nearly identical results to BD+36 4032. Table 4 summarizes the best-fit 1T APEC model. No significant fit improvement was obtained by adding a second temperature component. The N_H from Table 4 gives $A_V = 5.2$ [4.5 - 5.6] mag, in excellent agreement with the optically-determined value $A_V = 5.1$ mag (TF82). Thus, we find no excess X-ray absorption toward HD 229059.

4.3. Berkeley 87-4

This B0.2 III star lies $\approx 5.1'$ west of WR 142 and is object number 4 in the list of likely cluster members compiled by TF82. It was included in the study of Massey et al. (2001) who obtained a mass estimate $M_* = 23\ M_\odot$. Berkeley 87-4 was the third brightest *Chandra* X-ray detection of the OB stars in Berkeley 87 (Table 2). There are sufficient counts for a crude spectral fit, and a 1T APEC model gives N_H and kT values that are similar to the brighter OB stars BD+36 4032 and HD 229059 but a lower X-ray luminosity (Table 4). The X-ray derived N_H agrees to within the model uncertainties with that expected from optical reddening (TF82).

4.4. V439 Cyg

This variable star is also known as MWC 1015 and is object number 15 in the list of likely cluster members compiled by TF82. V439 Cyg has anomalous colors and is displaced well to the redward side of the zero-age main-sequence in the cluster color-magnitude diagram (TF82). The star's spectrum is peculiar and evidently variable, with most recent studies assigning an early B spectral type of B0e (Polcaro & Norci 1998) or B[e] (Massey et al. 2001). V439 Cyg shows some similarities to a LBV (Polcaro & Norci 1998).

V439 Cyg lies $\approx 3.2'$ NW of WR 142 and is a bright near-IR source with 2MASS data giving $K_s = 7.59$ mag and position 2MASS J202133.57+372451.57. There is no X-ray source at or near this position in our *Chandra* image. A circular region of radius 1.96″ (90% encircled

energy at E = 2 keV[11]) centered on the V439 Cyg 2MASS position encloses only one photon in the ACIS-I image (0.3 - 8 keV range).

To compute an X-ray upper limit, we assume a conservative 4-count ACIS-I detection threshold and an intrinsic thermal stellar spectrum similar to the two OB stars discussed above. Using $N_H = 1.0 \times 10^{22}$ cm^{-2} corresponding to E(B−V) = 1.53 (TF82) and a Raymond-Smith solar-abundance thermal plasma model with kT = 0.6 keV, the *Chandra* PIMMS[12] simulator gives an unabsorbed flux upper limit $F_X(0.3 - 8 \text{ keV}) \leq 3.9 \times 10^{-15}$ ergs cm^{-2} s^{-1}. If V439 Cyg is a cluster member, then d = 1.23 kpc gives log $L_X \leq 29.85$ (ergs s^{-1}).

Given the unusual nature of V439 Cyg, further consideration of its X-ray non-detection is warranted. In this regard, it is important to note that *Chandra* detected only the most luminous B stars in the cluster having absolute magnitudes $m_V \leq -2.1$ (Sec. 4.5). Several less-luminous early B stars were undetected (Table 2 notes). This is likely a consequence of the known $L_X \propto L_{bol}$ trend for O and early B-type stars (Berghöfer et al. 1997). The absolute magnitude of V439 Cyg is not well-known due to uncertain reddening, but it appears to lie at or near the m_V cutoff for our *Chandra* detections (Figure 7 of TF82). Thus, V439 Cyg may have insufficient L_{bol} to produce an X-ray luminosity above the *Chandra* detection threshold.

Excess absorption toward V439 Cyg may have also partially contributed to its non-detection. The anomalous colors of V439 Cyg imply excess reddening, and it may be surrounded by a shell of material that was ejected during a previous mass loss phase (Polcaro & Norci 1998). A gas-rich shell would increase the line-of-sight photoelectric absorption to lower energy X-rays (E < 1 keV).

If V439 Cyg is indeed a LBV (Polcaro & Norci 1998), it could be evolving into the WN phase. For stars of initial masses ∼ 40 - 75 $M_\odot$, the evolutionary sequence is (Crowther 2007): O → LBV → WN_{H-poor}. Some putatively single WN7-9 stars (also known as WNL stars) have so far gone undetected in X-rays (Figure 5). But a few recent WNL detections have been reported, including an unambiguous detection of the apparently single WN9ha star WR79a (Skinner et al. 2010b), a possible faint detection of WR 16 (WN8h) in a recent *XMM-Newton* observation (Figure 5), and a new *Chandra* detection of the WN8 component of the close WR+OB binary system WR 147 (Zhekov & Park 2010). Although the nature and evolutionary status of V439 Cyg remain somewhat of a mystery, its X-ray non-detection

[11]http://cxc.harvard.edu/cal/Acis/Cal_prods/psf/eer_on.html.

[12]For information on PIMMS (Portable Interactive Multi-Mission Simulator) see http://cxc.harvard.edu/ciao/ahelp/pimms.html.

would not be in discord with an evolved star that is approaching the WNL phase, given that a few other WNL stars have also gone undetected in X-rays.

4.5. Other B Stars in Berkeley 87

In addition to the OB stars discussed above, *Chandra* provides faint X-ray detections of four other B stars in Berkeley 87. These are Berkeley 87 no. 13 (B0.5 III), no. 24 (B1 Ib), no. 26 (B0.5 Iab), and no. 32 (B0.5 III). Their basic properties are summarized in Table 2, but they lack sufficient counts for spectral analysis. We also report non-detections of seven other B stars in Berkeley 87 (Table 2 notes).

The *Chandra* results show a noticeable trend in that all of the B star detections have high luminosities ($m_V \leq -2.1$; TF82 photometry). Most, but not all, of the undetected B stars are less luminous ($m_V \geq -2.1$). However, there are a few interesting exceptions. The B1 V star Berkeley 87-31 ($m_V = -2.7$; TF82) lies nearly on-axis at an offset of 18.7″ from WR 142 but was not detected. However, it does lie near an ACIS-I CCD gap. Two other luminous but undetected B stars, no. 9 (B0.5 V) and no. 38 (B2 III), lie further off-axis (3.9′ and 5.0′, respectively).

5. Discussion

5.1. Excess X-ray Absorption Toward WR 142

Chandra spectral fits of WR 142 (Table 3) give an absorption column density of $N_H \approx 4$ - 5×10^{22} cm^{-2}. In contrast, optical studies yield $N_H \approx 1 \times 10^{22}$ cm^{-2} (TF82, Barlow & Hummer 1982, van der Hucht 2001, Gorenstein 1975 conversions) for Berkeley 87 cluster members. Our X-ray analysis of the cluster members BD+36 4032 and HD 229059 (Sec. 4) also yields $N_H \approx 1 \times 10^{22}$ cm^{-2}. Thus, the X-ray spectra clearly show that excess absorption is present toward WR 142 that is not seen toward two other massive cluster members. This could arise either in the dense WO wind or perhaps in cold circumstellar gas.

Excess X-ray absorption seen as a disagreement between absorption based on optical extinction and the X-ray fit N_H has been seen in other WR stars as well, such as γ Vel[2] (Skinner et al. 2001) and recently detected WN stars (Skinner et al. 2010b).

Inhomogeneous extinction, although present, does not account for the discrepancy in X-ray and optical N_H values for WR 142. The spread in extinction values for cluster members is small, from $N_H = (0.8$ - $1.3) \times 10^{22}$ cm^{-2} (TF82, Gorenstein 1975 conversion). Additionally,

the smallest foreground extinction is near the south and WR 142 is $\approx 2.6'$ southeast of the cluster center (TF82), indicating the excess N_H is due to local absorption associated with WR 142.

If the excess absorption is due to the wind, we can estimate the radius at which the X-rays emerge using a wind optical depth calculation. From the observed *Chandra* WR 142 spectrum, the X-rays are entirely absorbed below ≈ 2 keV. Using generic WO abundances (van der Hucht et al. 1986) and assuming the mass- loss parameters in Table 1, the radius of optical depth unity at E = 2 keV is $R(\tau = 1,\ 2\ \mathrm{keV}) \approx 1500\ R_\odot$. Clumping in the WR winds may reduce the mass loss rate by a factor of 2 - 4 (Crowther 2007) and would reduce $R(\tau = 1,\ 2\ \mathrm{keV})$ by the same factor. $R(\tau = 1)$ is well outside the wind acceleration zone and the wind will already have reached terminal speed, assuming a standard $\beta = 0.5$ - 1.0 wind velocity law. It should be kept in mind that this is a *minimum* radius for 2 keV X-rays to escape.

Another possibility regarding excess absorption is the presence of cold circumstellar gas. Nebulosity around WR 142 has been detected (Miller & Chu 1993), though a ring nebula is not present. Polcaro et al. (1997) note excess reddening surrounding WR 142 of at least $N_H = 2.7 \times 10^{21}$ cm^{-2} (Gorenstein 1975 conversion) suggesting dense material, possibly a nebula from the stellar wind. Alternatively, Lozinskaya (1991) detected a distant IR shell (~ 23 pc from WR 142) whose dynamical age suggests that it formed before, and therefore independently, of the WO wind. Though it is apparent that some circumstellar material is present, our X-ray spectral fits have not distinguished between wind absorption and absorption by circumstellar gas far from the star. Both the wind and local circumstellar material could contribute to the excess X-ray absorption.

5.2. Is WR 142 a Binary?

There is no evidence from ACIS images (or other observations) that WR 142 is a binary. For an on-axis point source, the *Chandra* HRMA and ACIS PSF encircles 70% of the source energy for an angular source radius of $\approx 1.2''$ at 2 keV and $\approx 1.3''$ at 6 keV[13]. If two X-ray sources are present, their separation must be $<1''$.

The WR 142 X-ray luminosity from this *Chandra* observation is much less than that of known WR+O binaries, which are generally very luminous in the X-rays. Due to plasma formed in colliding wind shocks, these systems can have luminosities approaching $L_X \approx 10^{33}$

[13]http://cxc.harvard.edu/cal/Acis/Cal_prods/psf/eer_on.html.

ergs s^{-1}, such as γ^2 Vel (WC8+O7.5III; Skinner et al. 2001, Schild et al. 2004). WR 142 is at least two orders of magnitude less luminous.

However, the possibility of an unseen companion remains. But, a compact companion seems to be unlikely. Theoretical models of the WR winds accreting onto neutron stars predict high luminosity log $L_X > 34$ (ergs s^{-1}) (HD 50896 = EZ CMa, Stevens & Willis 1988). Additionally, a neutron star would be required to spin fast enough to throw off most of the accreting material to remain undetected (propeller effect, e.g. Lipunov 1982). If an optically faint lower mass normal stellar companion (rather than a compact object) lies close to WR 142, it could easily escape detection.

Currently, the binary frequency for galactic WR stars is ∼40% (van der Hucht 2001). Additional searches for binarity are needed for WR 142. These could include high resolution infrared imaging or radio interferometry, though they would only be capable of detecting a companion down to separations of a few tenths of an arcsecond. More promising approaches would be to search for periodic photometric or spectroscopic variability that could signal a closer spectroscopic companion. Spectroscopically, an X-ray emitting companion orbiting in the WR wind could reveal itself through phase variability of the WR star ultraviolet lines (Hatchett & McCray 1977).

5.3. Thermal versus Nonthermal Emission

Low counts in the WR 142 ACIS-I spectrum result in nearly identical fits by either thermal APEC models or power-law models. As such, the WR 142 spectrum cannot sufficiently distinguish between a very high temperature thermal plasma and nonthermal processes e.g. inverse Coulomb scattering due to relativistic electrons accelerated in wind shocks (Chen & White 1991a). In general, other WR stars with higher signal-to-noise spectra show detections of emission lines indicative of thermal emission. While the goodness-of-fit for spectral models slightly improves with the addition of the Fe K line for WR 142, there are not enough line counts to qualify as a definite line detection. There is no obvious evidence of other thermal emission lines, such as the S line at 2.46 keV. Theoretical models do exist that attempt to account for the hard X-ray emission from some early type stars by nonthermal processes (Chen & White 1991a). However, if WR 142 were a nonthermal X-ray source, it would be the first putatively single WR star in that class. The possibility of nonthermal emission has been previously mentioned for other WR stars such as WR 110 but the evidence for nonthermal emission was not conclusive (Skinner et al. 2002).

5.4. Thermal Emission Mechanisms

Thermal X-ray emission is possible through several processes. Often radiative wind shocks are considered, yet with no emission below 2 keV detected from WR 142, a line-driven flow instability model predicting soft X-rays from radiative wind shocks that is typically assumed for O stars (Gayley & Owocki 1995) cannot explain the hard emission. We discuss wind kinetic energy conversion, colliding wind shocks, magnetically confined wind shocks (MCWS), and coronal emission as possible thermal emission processes.

5.4.1. Kinetic Energy of the Wind

Due to the extreme mass loss rate, the kinetic energy in the wind of WR 142 is enough to account for the X-ray luminosity. The kinetic energy of the wind supplies log $L_{wind} \approx$ 38.2 (ergs s^{-1}) which is much greater than the X-ray luminosity observed of log $L_X \approx 31$ (ergs s^{-1}). The effects of clumping in the wind on the mass loss rate would not change this conclusion, reducing log L_{wind} by 0.6 dex (ergs s^{-1}) at most. Thus even if the efficiency for converting the wind kinetic energy into X- rays were small, the wind still could supply the energy.

5.4.2. Colliding Wind Shocks

Because WR 142 has no known companion, a colliding wind shock model does not obviously apply. However, such models could explain the high temperatures of the X-ray emission produced from the high wind speed of WR 142. Assuming $v_\perp \approx v_\infty = 5500$ km/s (Kingsburgh et al. 1995), the maximum X-ray temperature from a colliding wind shock (eq. 1 of Luo et al. 1990) would be $kT_{max} \approx 1.95$ keV μ $[v_\perp/$ (1000 km/s^{-1})$]^2 \geq 59$ keV for WR 142. The symbol μ is the mean atomic (ionic) weight per particle (ions + electrons). This approximation does not assume specific WO-type wind abundances (though $\mu \geq 1$ for WR stars), but shows that a colliding wind shock onto an unseen companion or its wind could explain the high temperatures indicated by APEC spectral fits.

If we assume a B0V companion with a radius $R_* = 7.4$ R$\odot$ (Allen 1976), we find a separation of ≈ 1 AU is required to produce the observed *Chandra* X-ray luminosity through colliding wind shocks (eq. 81 of Usov 1992). If we account for clumped winds, the separation scales as $\dot{M}^{1/2}$ and would reduce to 0.7 AU if the mass loss rate is reduced by a factor of 2. At a distance of 1.23 kpc, a 1 AU separation between WR 142 and its hypothetical companion would produce an angular separation of much less than $1''$ (≈ 1 mas) and would

not be resolvable by *Chandra*. However, this separation is smaller than the escape radius for X-rays, which is 375 - 1500 R$\odot$ (Section 5.1). A favorable orbital phase and geometry with the wind blown cavity around the companion along our line of sight would allow for the X-rays to escape (e.g. as occurs in γ^2 Vel; Schild et al. 2004), especially with clumped winds. To consider shock emission from the fast winds impacting circumstellar material, more information on the CS material's density, geometry, and distance from WR 142 would be necessary.

5.4.3. Magnetically Confined Wind Shocks

For luminous stars, a surface magnetic field may be able to channel wind flow into shock collisions with sufficient velocity to produce hard X-ray emission. Generally, the magnetic field lines are thought to bend radiatively driven winds towards the magnetic equator, where the hemispheric winds collide. Such magnetically-confined wind theories have been used to explain X-ray emission for magnetic Ap-Bp stars (Babel & Montmerle 1997a) and young O-type stars (Babel & Montemerle 1997b, θ Ori C in Gagné et al. 2005). The winds were not radiatively driven in the Ap-Bp model but the resulting shocks are unaffected. We can determine the minimum magnetic field strength necessary to confine the winds in comparison to the wind magnetic confinement parameter using equation 7 of ud-Doula & Owocki (2002), which is dependent upon the mass loss rate, v_∞, and radius of the star. We approximate the radius of WR 142 to be one solar radius (Abbott et al. 1986). We find that B $\approx \sqrt{\eta_*}$ 20 kG at the stellar surface. Here, η_* is the wind magnetic confinement parameter and is 1 for marginal confinement, 10 for strong confinement that produces shocks strong enough to produce 1 keV emission (ud-Doula & Owocki 2002). Wind clumping could reduce the minimum magnetic field strength by a factor of $\sqrt{2}$ to 2. It remains to be shown that WR stars have such strong magnetic fields.

Additionally, it can be shown that the maximum temperature at the shock front from MCWS could reach maximum temperatures of tens of keV (eq. 4 of Babel & Montmerle 1997a) for high-velocity ionized metal-rich winds ($\mu \geq 1.33$) such as that of WR 142. The highest temperature is only possible at the shock front and will drop off to lower temperatures for most of the shocked plasma, but still easily could explain the observed hard emission from WR 142. It is important to note though that MCWS theories have not yet been extended to WR stars, where several problems such as larger mass loss rates have not yet been addressed. Additionally, a magnetic rotator model with modulated the winds was invoked to explain the periodic variations of the X-ray emission from θ^1 Orionis C (Babel & Montmerle 1997b) but WR 142 here shows no such periodic X-ray emission or B-field detection so far.

5.4.4. Coronal Emission

As suggested for some OB stars, X-rays could be formed in a thin corona at the base of the wind (e.g. Cassinelli & Olson 1979). However, our calculations suggest that the kT $\approx$ 2 keV X-rays emerge from very large radii, roughly r $\gtrsim$ 1000 R_*, assuming a spherical homogenous wind. This is too far out to be attributed to a corona. Also, X-ray variability would be expected with coronal emission as magnetic (coronal) emission is usually associated with short-term X-ray variability (e.g. flares). No significant variability or flaring was detected in the *Chandra* observation.

5.5. Nonthermal Emission Processes

Electrons in the stellar wind accelerated to relativistic energies by the Fermi mechanism and trapped in weak magnetic fields could scatter stellar UV photons to produce X-ray emission and γ-ray emission (Chen & White 1991a, b), as suggested for WR stars by Pollock (1987). The accelerated electrons undergo adiabatic cooling between shocks and thus can only lose heat through nonthermal processes, such as inverse Compton, nonthermal bremsstrahlung, or synchrotron radio emission (Chen & White 1991a). Such processes may be at work in WR 142: X-ray spectra of WR 142 can be fitted with a power-law and Berkeley 87 lies close to an extended region of high-energy γ-ray emission in Cygnus (Abdo et al. 2007, 2009; Smith et al. 2005), though the primary source of the γ-ray emission has not yet been proven to be Berkeley 87 itself.

For OB stars, the radiation will produce a power-law electron spectrum where the X-ray flux from inverse Compton emission should scale with energy as $F_X \propto E^{-1/2}$ for electron index n = 2 (Chen & White 1991a). Spectral fits in Table 3, when the given photon index $\Gamma_{pow} = 1$ is converted to an energy index, give $F_X \propto E^0$, though the photon index was poorly constrained. If the photon index is frozen to $\Gamma = 1.5$ so as to produce Chen & White's energy power-law index, the fit is reasonable but exhibits slightly more absorption and higher X-ray flux and luminosity (Table 3 footnotes).

The X-ray emission is predicted to be hard without large scale variations, and if present, variations only on timescales of hours to days (Chen & White 1991a). However, the Chen & White (1991a) model is tuned to OB stars, such that inverse Compton is the assumed emission mechanism whereas bremsstrahlung may be just as important or even dominate inverse Compton for WR stars. Additionally, other factors, such as the coulomb effects in the dense WR wind, have not been fully evaluated (Chen & White 1991a). Still, the nonthermal emission process is plausible for some WR stars, especially where nonthermal radio emission

is detected (Pollock 1987). WR 142, is as of yet, undetected in the radio. Cappa et al. (2004) determined an upper limit of <0.90 mJy for the 3.6 cm flux density from WR 142. Despite a lack of detection of nonthermal radio emission at 3.6 cm, radio observations at longer wavelengths where nonthermal emission could lead to higher flux densities would be useful. The hard and essentially featureless X-ray spectrum of WR 142 could be nonthermal, but a higher signal-to-noise X-ray spectrum will be needed to distinguish between thermal and nonthermal emission.

6. Comments on Wolf-Rayet Star X-ray Emission

The X-ray detection of WR 142 presents a major question: why don't we observe X-rays from the WC subtype when we detect hard emission from a WO star? When plotting L_{bol} versus L_X, WR 142 lies in the region occupied by undetected WC stars (Figure 5). WOs are more evolved than WCs, and WO winds are even more metal-rich and should thus be more efficient absorbers of soft X-rays.

However, WR 142 has a very high terminal wind speed and a very high effective temperature (T_{eff}) compared to WC stars (Crowther 2007). A higher effective temperature would lead to a more fully ionized wind, which lowers the wind opacity (κ) to X-rays (see eq. 6 of Ignace et al. 2000). The higher wind speed leads to a smaller radius of optical depth unity for X-rays of a given energy where $R(\tau = 1, E) = \dot{M}/(4\pi v_\infty) \times \kappa\ (E)$ (eq. 9 of Ignace et al. 2000). In the case for WR 142, the terminal wind speed is greater and the wind opacity may be smaller than for WC stars, leading to a smaller $R(\tau = 1, E)$. Thus, X-rays may be able to escape from smaller radii closer to the star, which could explain why WR 142 has been detected in the X-rays but why WC stars have (so far) not been detected.

Another possible explanation is that WR 142 is not a single star (see Section 5.2). Some WC stars that are members of binary systems have been known to display hard X-ray emission (e.g. γ^2 Vel, WC8+O7.5) but the X-ray emission from WR 142 is much less luminous. WR+O binaries display much stronger emission. Perhaps X-ray emission from a binary decreases as a WR star evolves from WN to WC to WO because of changes within the star or its wind. Maybe the luminosity difference lies in evolution of the unseen companion star. WR 142, if a binary, may not have an O star companion but some other less massive non- degenerate stellar companion. As discussed in Section 5.4.2, a close companion at the right separation could account for a lower X-ray luminosity using a colliding wind model.

The hard X-ray emission and fast wind from WR 142 may indicate a colliding wind shock that could be explained by an as of yet undetected companion at close separation, such as a

B0V star companion at $\sim$ 1 AU from WR 142 (Section 5.4.2). This close separation would not be resolved by *Chandra*. If a less massive unseen companion is present, then *Chandra* may be observing colliding wind shock emission at or near the surface of the companion (Usov 1992) and no intrinsic emission from the stars themselves. Even if the undetected companion star had no wind itself, the overwhelming wind from WR 142 would shock onto the companion's surface and produce the same effect. For example, a colliding wind shock onto a less massive companion could occur if the companion were an X-ray faint B- or A-star and any intrinsic X-ray emission from WR 142, if any exists, were completely absorbed, e.g. by its wind. If this is the case, then we do not detect X-ray emission from WR 142 itself and there is no contradiction with non-detections of single WC stars.

Another thought to consider could involve the very high wind speeds of WR 142. What if the winds give rise to some exotic nonthermal emission processes, such as proposed by Chen & White (1991a), that do not get triggered in WR stars with lower terminal wind speeds or lower $T_{\rm eff}$? The detection of X-rays from the WO type WR 142 may even suggest that the absence of X-rays from WC type stars be considered tentative until sensitive observations of a larger sample of WC stars are obtained.

7. Conclusions

1. *Chandra* has detected hard, heavily-absorbed X-ray emission from the rare WO-type star WR 142. No soft emission below 2 keV was detected by *Chandra*.

2. The observed X-ray flux is consistent with the flux from a previous *XMM-Newton* observation, within the uncertainties, and no significant X-ray variability was detected during the *Chandra* observation.

3. Due to the faint emission from WR 142, lack of prominent emission lines, and low numbers of counts, statistics are unable to distinguish between thermal and nonthermal X-ray emission mechanisms when fitting the spectrum and both have been considered. If the emission is thermal, very high plasma temperatures are inferred.

4. In addition to WR 142, *Chandra* detected seven luminous OB stars in Berkeley 87, while eight other B stars were undetected. The hard X-rays and excess absorption of WR 142 contrast with two X-ray bright OB stars in Berkeley 87, which display predominately soft X-ray emission and absorptions consistent with optical values.

5. Though the X-ray emission mechanism in WR 142 is unclear, the hard X-ray spectrum observed by *Chandra* could be explained by a colliding wind shock onto an as yet

unseen companion, though the escape of the X-rays may require a geometry with the companion in front of WR 142. A colliding wind shock interpretation would also resolve an apparent contradiction of non-detections in the X-rays of single WC stars while WR 142 (a WO star) was detected. A key point not to be overlooked is that colliding winds can produce very hot plasma (as observed) even in the absence of magnetic fields.

6. Alternatively, mechanisms that assume stellar magnetic fields such as MCWS or inverse Compton scattering (as formulated by Chen & White 1991a) could play a role in the X-ray emission of WR 142. However for MCWS, very strong surface fields of tens of kG would be required to effectively confine the powerful WR 142 wind (Sec. 5.4.3), also noted by Oskinova et al. (2009) in their MCWS interpretation. There is so far no observational evidence of such strong B-fields in WR stars, nor do the existing X-ray data show any obvious signatures of impulsive X-ray flares that often accompany magnetic reconnection. If WR 142 has even a weak surface magnetic field, then X-ray production via inverse Compton scattering provides an attractive alternative to the extreme conditions required for magnetic wind confinement. A key question is whether the X-ray spectrum of WR 142 is indeed a power-law, as expected for inverse Compton scattering. To answer this question, a higher signal-noise X-ray spectrum from a much deeper observation will be required.

This work was supported by *Chandra* award GO9-0004X issued by the Chandra X-ray Observatory Center (CXC). The CXC is operated by the Smithsonian Astrophysical Observatory (SAO) for, and on behalf of, the National Aeronautics Space Administration under contract NAS8-03060. We have utilized NASA's Astrophysics Data System Service and the SIMBAD database. This research has made use of data obtained from the High Energy Astrophysics Science Archive Research Center (HEASARC), provided by NASA's Goddard Space Flight Center.

REFERENCES

Abbott, D.C., Bieging, J.H., Churchwell, E., & Torres, A.V., 1986, ApJ, 303, 239

Abdo, A.A. et al., 2007, ApJ, 658, L33

Abdo, A.A. et al., 2009, ApJ, 700, L127

Allen, C.W., 1976, Astrophysical Quantities (3rd ed.), (London: Athlone Press)

Anders, E., & Grevesse, N., 1989, Geochim. Cosmochim. Acta, 53, 197

Argon, A.L., Reid, M.J., & Menten, K.M., 2000, ApJS, 129, 159

Babel, J., & Montmerle, T., 1997a, A&A, 323, 121

Babel, J., & Montmerle, T., 1997b, ApJ, 485, L29

Barlow, M.J., & Hummer, D.G., 1982, IAUS, 99, 387

Barlow, M., 1991, in 143rd Symp. of the IAU, *Wolf-Rayet Stars and Interrelations with Other Massive Stars in Galaxies*, ed. K.A. van der Hucht & B. Hidayat (Netherlands: IAUS 143), 281

Baum, E., Hamann, W.-R., Koesterke, L., & Wessolowski, U., 1992, A&A, 266, 402

Berghöfer, T.W., Schmitt, J.H.M.M., Danner, R., & Cassinelli, J.P., 1997, A&A, 322, 167

Cappa, C., Goss, W.M., & van der Hucht, K.A., 2004, AJ, 127, 2885

Cash, W., 1979, ApJ, 228, 939

Cassinelli, J.P., & Olson, G.L., 1979, ApJ, 229, 304

Chen, W., & White, R.L., 1991a, ApJ, 366, 512

Chen, W., & White, R.L., 1991b, ApJ, 381, L63

Conti, P.S., Garmany, C.D., de Loore, C., & Vanbeveren, D., 1983, ApJ, 274, 302

Crowther, P.A., Orsola De Marco, & Barlow, M.J., 1998, MNRAS, 296, 367

Crowther, P.A., 2007, ARA&A, 45, 177

Gagné, M., Oksala, M.E., Cohen, D.H., Tonnesen, S.K., ud-Doula, A., Owocki, S.P., Townsend, R.H.D., & MacFarlane, J.J., 2005, ApJ, 628, 986

Gayley, K.G., & Owocki, S.P., 1995, ApJ, 446, 801

Georgy, C. Meyet, G., Walder, R., Folini, D., & Maeder, A., 2009, A&A, 502, 611

Gorenstein, P., 1975, ApJ, 198, 95

Gregory, P.C., & Loredo, T.J., 1992, ApJ, 389, 146

Gregory, P.C., & Loredo, T.J., 1996, ApJ, 473, 1059

Hamann, W.-R., Gräfener, G., & Liermann, A., 2006, A&A, 457, 1015

Hatchett, S., & McCray, R., 1977, ApJ, 211, 552

Heinrich, J., 2003, in Statistical Problems in Particle Physics, Astrophysics, & Cosmology, ed. L. Lyons, R. Mount, & R. Reitmeyer (eConf C030908), 52, http://www.slac.stanford.edu/econf/C030908/ proceedings.html

Ignace, R., Oskinova, L.M., & Brown, J.C., 2003, A&A, 408, 353

Ignace, R., Oskinova, L.M., & Foullon, C., 2000, MNRAS, 318, 214

Kingsburgh, R.L., Barlow, M.J., & Storey, P.J., 1995, A&A, 295, 75

Lipunov, V.M., 1982, Sov. Astron. Lett., 8, 194

Lozinskaya, T.A., 1991, in 143rd Symp. of the IAU, *Wolf-Rayet Stars and Interrelations with Other Massive Stars in Galaxies*, ed. K.A. van der Hucht & B. Hidayat (Netherlands: IAUS 143), 365

Luo, D., McCray, R., & Mac Low, M.-M., 1990, ApJ, 362, 267

MacFadyen, A.I., & Woosley, S.E., 1999, ApJ, 524, 262

Massey, P., DeGioia-Eastwood, K., & Waterhouse, E., 2001, AJ, 121, 1050

Matthews, H.E., Goss, W.M., Winnberg, A., & Habing, H.J., 1973, A&A, 29, 309

Miller, G.J., & Chu, Y.-H., 1993, ApJS, 85, 137

Oskinova, L.M., 2005, MNRAS, 361, 679

Oskinova, L.M., Hamann, W.-R., Feldmeier, A., Ignace, R., & Chu, Y.-H., 2009, ApJ, 693, L44

Oskinova, L.M., Ignace, R., Hamann, W.-R., Pollock, A.M.T., & Brown, J.C., 2003, A&A, 402, 755

Polcaro, V.F., Giovannelli, F., Manchanda, R.K., Norci, L., & Rossi, C., 1991, A&A, 252, 590

Polcaro, V.F., & Norci, L., 1998, A&A, 339, 75

Polcaro, V.F., Viotti, R., Rossi, C., & Norci, L., 1997, A&A, 325, 178

Pollock, A.M.T., 1987, A&A, 171, 135

Postnov, K.A., & Cherepashchuk, A.M., 2001, Astron. Rep., 45, 517

Press, W.H., Teukolsky, S.A., Vetterling, W.T., & Flannery, B.P., 1992, Numerical Recipes in Fortran: The Art of Scientific Computing (2nd ed.; New York: Cambridge Univ. Press), 617

Sanduleak, N., 1971, ApJ, 164, L71

Schild, H. et al., 2004, A&A, 422, 177

Skinner, S.L., Güdel, M., Schmutz, W., & Stevens, I.R., 2001, ApJ, 558, L113

Skinner, S., Güdel, M., Schmutz, W., & Zhekov, S., 2006, Ap&SS, 304, 97

Skinner, S.L., Sokal, K.R., Zhekov, S.A., Güdel, M., & Schmutz, W., 2010a, BAAS, 42, 567

Skinner, S.L., Zhekov, S.A., Güdel, M., & Schmutz, W., 2002, ApJ, 572, 477

Skinner, S.L., Zhekov, S.A., Güdel, M., & Schmutz, W., 2007, MNRAS, 378, 1491

Skinner, S.L., Zhekov, S.A., Güdel, M., Schmutz, W., & Sokal, K.R., 2010b, AJ, 139, 825

Smith, A.J. et al., 2005, ICRC, 4, 271

Smith, L.F., & Aller, L.H., 1969, ApJ, 157, 1245

Smith, L.F., Meynet, G., & Mermilliod, J.-C., 1994, A&A, 287, 835

Stephenson, C.B., 1966, AJ, 71, 477

Stevens, I.R., & Willis, A.J., 1988, MNRAS, 234, 783

Turner, D.G., & Forbes, D., 1982, PASP, 94, 789 (TF82)

Turner, D.G., Majaess, D.J., Lane, D.J., & Balam, D.D., 2010, BAAS, 42, 566

Turner, D.G., Rohanizadegan, M., Berdnikov, L.N., & Pastukhova, E.N., 2006, PASP, 118, 1533

ud-Doula, A., & Owocki, S.P., 2002, ApJ, 576, 413

Usov, V.V., 1992, ApJ, 389, 635

van der Hucht, D.A., Cassinelli, J.P., & Williams, P.M., 1986, A&A, 168, 111

van der Hucht, K.A., 2001, New A Rev., 45, 135

van der Hucht, K.A., 2006, A&A, 458, 453

Weidmann, W.A., Gamen, R., Díaz, R.J., & Niemela, V.S., 2008, A&A, 488, 245

Zhekov, S.A., & Park, S., 2010, ApJ, 709, L119

Table 1. Stellar Properties of WR 142

Parameter	Value	Notes[a]
Spectral Type	WO2	(1)(2)
Age (Myr)	$\sim$3 - 5	(3)
d (pc)	1230$\pm$40	(4)
V (mag.)	13.4	(2)
A_V (mag)	6.1	(5)
J,H,K_s (mag)	9.54,8.89,8.60	(6)
log $M/M_\odot$	0.9$\pm$0.2	(7)
$\dot{M}$ ($M_\odot$ yr^{-1})	1.7×10^{-5}	(8)
v_∞ (km s^{-1})	5500$\pm$200	(2)
log L_{wind} (ergs s^{-1})	38.2	(9)
log $L_{bol}/L_\odot$	5.35, 5.65	(10)

[a]Refs. and Notes: (1) Crowther et al. (1998) (2) Kingsburgh et al. (1995) (3) Massey et al. (2001), Polcaro & Norci (1998), Turner et al. (2010) (4) Turner et al. (2006) (5) van der Hucht 2001, using $A_V = 0.9A_v$ (6) 2MASS Point Source Catalog (7) Smith et al. (1994) (8) Unclumped value from Barlow (1991), Clumping could reduce $\dot{M}$ by a factor of $\approx$ 2 - 4 (Crowther 2007) (9) Polcaro et al. (1991), also $L_{wind} = (1/2)\dot{M}v_\infty^2$ (10) Determined by fitting photometric observations using a range of clumped mass loss rates, Oskinova et al. 2009

Table 2. X-ray Properties of WR 142 and OB stars[a] in Berkeley 87

Name	R.A. (J2000)	Decl. (J2000)	Net Counts (cts)	E_{25},E_{50},E_{75} (keV)	<E> (keV)	P_{const} KS/GL	Sp. Type	Identification (offset) (arcsec)
HD 229059	20 21 15.37	+37 24 31.2	341±19	1.09,1.36,1.67	1.54	0.40/0.93	B1 Ia[b]	HST 202115.36+372431.1 (0.16)[c]
Berkeley 87-4	20 21 19.26	+37 23 24.6	63±8	0.96,1.19,1.67	1.53	0.10/0.49	B0.2 III	HST 202119.25+372324.7 (0.16)
Berkeley 87-13	20 21 31.60	+37 20 40.6	5±2	...,1.25,...	1.60	0.55/...	B0.5 III	HST 202131.55+372041.4 (1.00)
Berkeley 87-24	20 21 38.21	+37 25 17.4	9±3	1.59,1.99,3.49	2.41	0.49/...	B1 Ib	HST 202138.33+372516.3 (1.80)
BD+36 4032	20 21 38.69	+37 25 15.4	254±16	1.08,1.34,1.64	1.43	0.01/0.62	O8.5 III[b]	HST 202138.68+372515.2 (0.23)
Berkeley 87-26	20 21 39.72	+37 25 05.6	11±3	0.92,1.09,1.78	2.00	0.70/...	B0.5 Iab	HST 202139.75+372505.9 (0.47)
WR 142	20 21 44.35	+37 22 30.7	46±7	2.99,4.28,5.32	4.31	0.77/0.40	WO2[d]	HST 202144.36+372230.5 (0.23)
Berkeley 87-32	20 21 47.35	+37 26 32.2	11±3	0.95,1.09,1.57	1.33	0.91/...	B0.5 III	HST 202147.35+372632.0 (0.18)

Note. — X-ray data using events in the 0.3 - 8 keV range within a 3σ *wavdetect* ellipse, which for WR 142 is ≈ 11.25 pix^2. Tabulated quantities are: J2000.0 X-ray position (R.A., decl.); net counts and net counts error from *wavdetect* (accumulated in a 70148 s exposure, rounded to the nearest integer, background subtracted and PSF-corrected); 25%, 50%, and 75% photon quartile energies (E_{25}, E_{50}, and E_{75}), mean photon energy (<E>); probability of constant count-rate determined by the Kolmogorov-Smirnov (KS) test and the Gregory-Loredo (GL) algorithm, where $P_{const} \leq 0.05$ would indicate likely variability; spectral type as indicated by SIMBAD or otherwise noted; and HST GSC candidate counterpart identification within a $2''$ search radius. The offset (in parentheses) is given in arc seconds between the X-ray and counterpart position. Ellipses indicate insufficient counts for reliable measurement.

[a]Faint B stars not detected: Berkeley 87 nos. 7 (B), 9 (B0.5 V), 15 (V439 Cyg, B0e/B[e] - references in Sec. 4.3), 16 (B2 V), 18 (B1 V), 31 (B1 V), 34 (B), and 38 (B2 III). Spectral types are from the SIMBAD database.

[b]Spectral type from Massey et al. (2001).

[c]Two close HST sources have nearly the same sexagesimal coordinates and are indistinguishable by *Chandra*.

[d]Spectral type references in Table 1.

Table 3. *Chandra* Spectral Fits for WR 142

Parameter			
Model	1T APEC	POWER	POWER + GAUSS
N_H (10^{22} cm^{-2})	5.66	4.61	4.55
kT (keV)	{20.}[a]	...	...
norm (10^{-13})	6.36	...	...
Γ_{pow}[b]	...	1.0 [c]	{1.0}
$norm_{pow}$ (10^{-6})	...	2.31	2.32
E_{line} (keV)	...	...	{6.67}
σ_{line} (keV)	...	...	{0.05}
$norm_{line}$ (10^{-8})	...	...	8.68
Abundances[d]	WO	...	...
C-statistic[e]	215.90	215.08	214.73
F_X (10^{-14} ergs cm^{-2} s^{-1})	1.65 (3.66)	1.74 (2.93)	1.77 (2.96)
$F_{X,line}$ (10^{-16} ergs cm^{-2} s^{-1})	...	...	8.66 (9.28)
log L_X (ergs s^{-1})	30.82	30.72	30. 73

Note. — Based on fits of ACIS spectra using XSPEC v12.5.0. The data were unbinned and not background subtracted (background is negligible). The tabulated parameters are absorption column density (N_H), plasma temperature (kT), XSPEC normalization (norm), photon power-law index (Γ_{pow}), power-law model normalization ($norm_{pow}$), Gaussian line centroid energy (E_{line}), line width (σ_{line} = FWHM/2.35), line normalization ($norm_{line}$). Quantities enclosed in curly braces were held fixed during fitting. WO abundances are from Table 1 of van der Hucht et al. (1986), except the hydrogen and nitrogen abundances are arbitrarily set to the small non-zero value 1×10^{-6} for compatibility with XSPEC. Solar values from Anders & Grevesse (1989) are used for any elements in the XSPEC abundance table that are not listed in van der Hucht et al. (1986). X-ray flux (F_X) is the observed (absorbed) value followed in parentheses by the unabsorbed value in the 0.3 - 8.0 keV range. The continuum-subtracted Gaussian line flux ($F_{X,line}$) is measured in the 6.5 - 6.9 keV range. X-ray luminosity (L_X) is the unabsorbed value in the 0.3 - 8.0 keV range. A distance of 1230 pc is assumed (Turner et al. 2006).

[a]If kT is allowed to vary, it runs away to the maximum temperature of 64. keV allowed by the APEC model. If frozen at a higher temperature of kT = 50 keV, the fit is similar and converges to $N_H = 5.38 \times 10^{22}$ cm^{-2}, C-statistic = 215.56, F_X = 1.67 (3.43) $\times 10^{-14}$ ergs cm^{-2} s^{-1}, and log L_X = 30.79 ergs s^{-1}.

[b]A photon index Γ_{pow} equates to $F_X \propto E^{-(\Gamma_{pow}-1)}$. That is, values of $\Gamma_{pow} > 1$ correspond to flux decreasing with increasing energy E.

[c]If the photon index is frozen to $\Gamma_{pow} = 1.5$, the fit gives $N_H = 5.91 \times 10^{22}$ cm^{-2}, C-statistic = 215.73, F_X = 1.64 (4.03) $\times 10^{-14}$ ergs cm^{-2} s^{-1}, and log L_X = 30.86 ergs s^{-1}.

[d]Varying the abundances did little to improve fits.

[e]Regrouped spectra to a minimum of 6 counts per bin enabled the use of χ^2 statistics. For 1T APEC models, this yielded a lower 90% confidence bound on kT>3.6 keV. 90% bounds on N_H were in the range [2.8 - 9.6] $\times 10^{22}$ cm^{-2} for models frozen at kT = 20 keV. We were not able to find stable confidence bounds on Γ_{pow} for the power-law models.

Table 4. *Chandra* Spectral Fits for X-ray Bright OB Stars

Parameter	BD+36 4032	HD 229059	Berkeley 87-4
Model	1T APEC	1T APEC	1T APEC
Abundances	solar	solar	solar
N_H (10^{22} cm^{-2})	1.13 [0.99 - 1.45]	1.16 [1.01 - 1.24]	0.82 [0.59 - 1.16]
kT (keV)	0.56 [0.35 - 0.69]	0.64 [0.47 - 0.81]	0.54 [0.27 - 0.74]
norm (10^{-4})	1.16 [0.69 - 4.31]	1.47 [0.76 - 1.75]	0.20 [... - 1.51]
χ^2/dof	23.7/18	30.7/28	2.8/4
χ^2_{red}	1.32	1.10	0.70
F_X (10^{-13} ergs cm^{-2} s^{-1})	0.20 (2.91)	0.32 (3.93)	0.05 (0.53)
log L_X (ergs s^{-1})	31.72	31.85	30.98

Note. — Based on fits of ACIS spectra binned to a minimum of 10 counts per bin using XSPEC v12.5.0. Square brackets enclose 90% confidence intervals. An ellipsis means the algorithm used to compute 90% confidence limits did not converge. The X-ray flux is the absorbed value, followed in parentheses by the unabsorbed value. A distance of 1.23 kpc is assumed. Solar abundances are from Anders & Grevesse (1989).

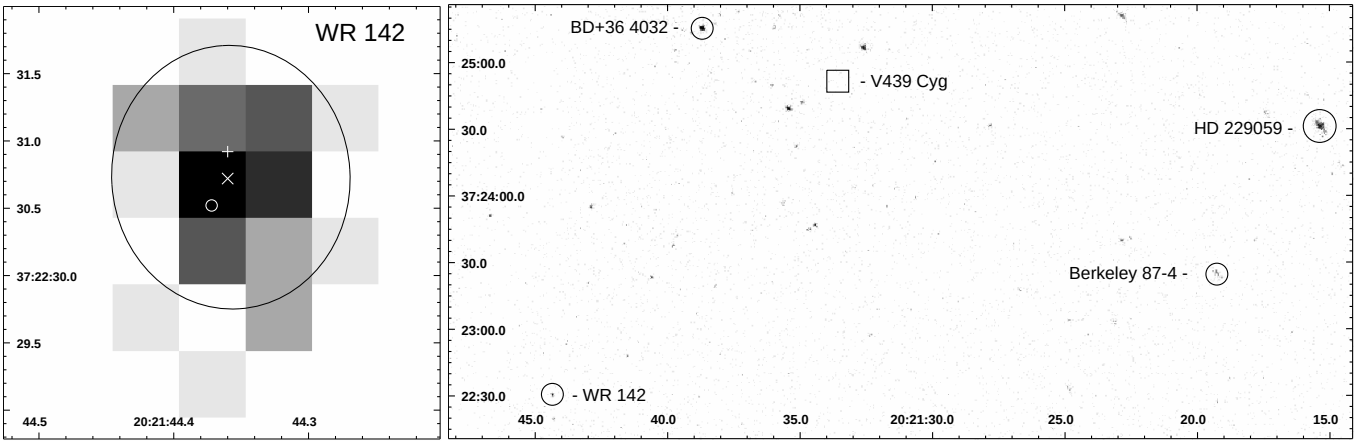

Fig. 1.— Left: An ACIS-I image (0.3 - 8 keV, log intensity scale) centered near WR 142. Indicators give the WR 142 position as follows: circle marks HST GSC 2.3.2 (optical), plus marks USNO-B1.0 (optical), and the cross marks both the *Chandra* and 2MASS (near-infrared) positions. WR 142 was only 28″ from the aimpoint. The 3σ ellipse determined by *wavdetect* is shown and encloses 46 ± 7 net counts. Right: An ACIS-I wide field image (0.3 - 8 keV, log intensity scale) showing the X-ray bright OB stars relative to WR 142, where circles mark the *Chandra* positions and the square marks a 2MASS position for the non-detection of V439 Cyg. All coordinates are J2000.0 and pixels are 0.492″.

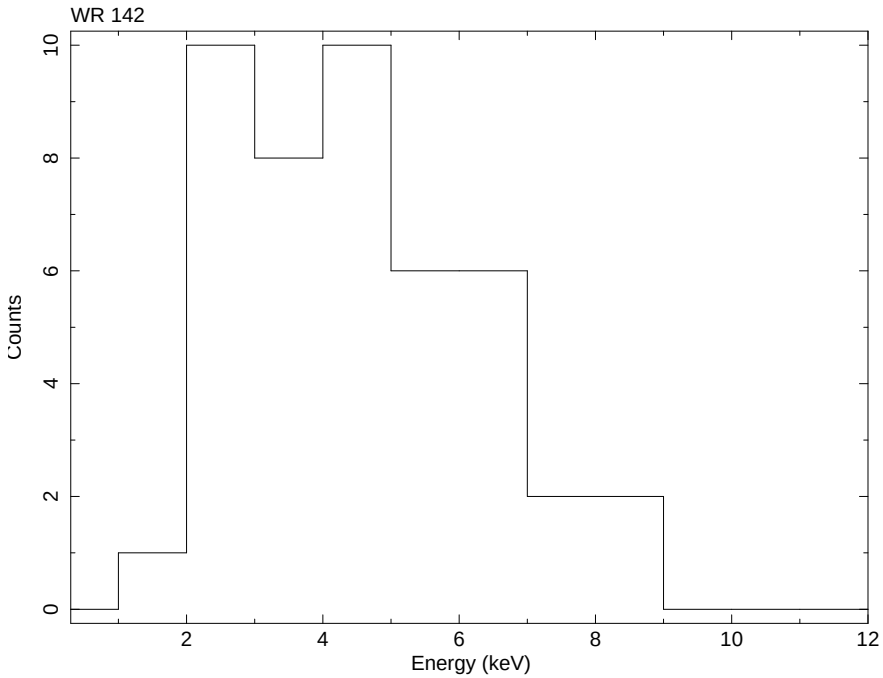

Fig. 2.— A histogram showing the observed X-ray event energies for WR 142 in the energy range from 0.3 - 12 keV (*wavdetect* 3σ ellipse extraction region). The bin size is 1 keV.

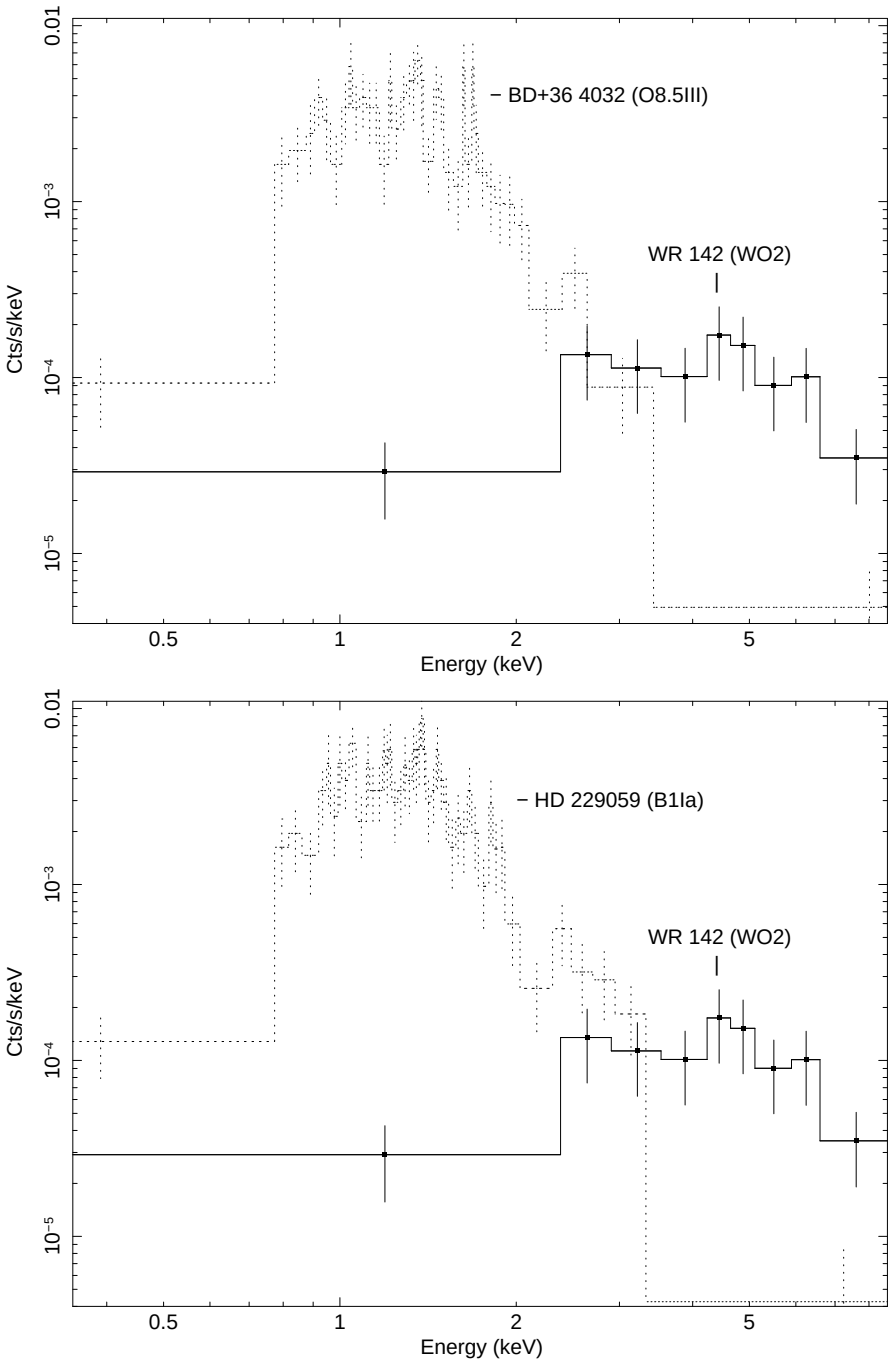

Fig. 3.— *Chandra* ACIS-I spectra of WR 142 (46 counts) and OB stars, top: the O8.5 III star BD+36 4032 (249 counts), bottom: the B1 Ia star HD 229059 (341 counts). Spectra were rebinned to a minimum of 5 counts per bin. The straight lines between data points are a histogram and not a fitted model. The spectra show a clear contrast. The WR 142 spectrum is dominated by hard emission above 2 keV while soft emission below 2 keV dominates the OB stars.

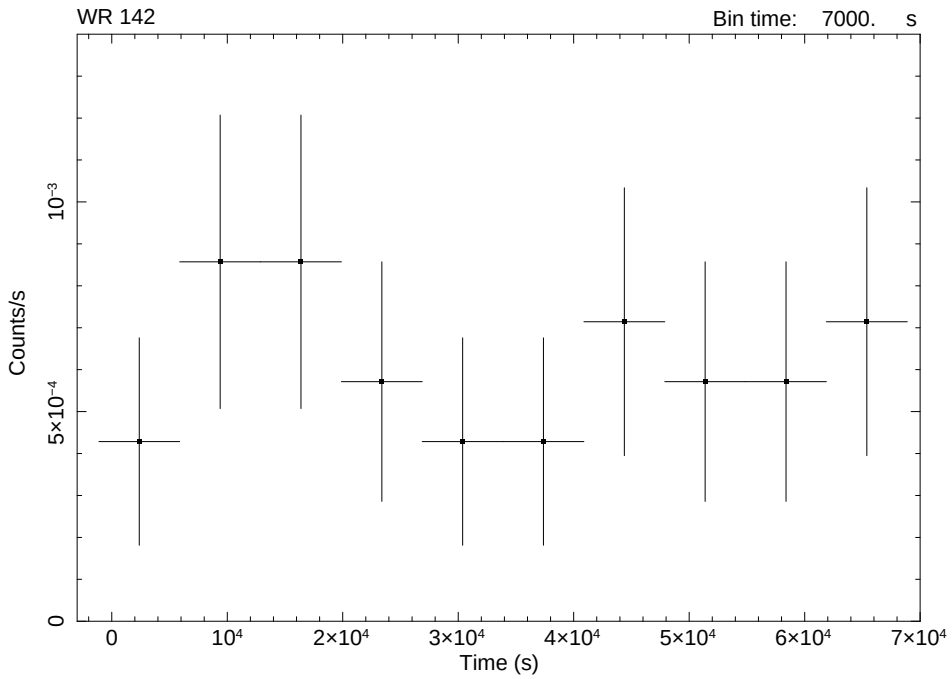

Fig. 4.— A *Chandra* lightcurve for WR 142 in the 0.3 - 8 keV energy range (1σ error bars). The extraction region was a 3σ ellipse (Figure 1) given by *wavdetect* output.

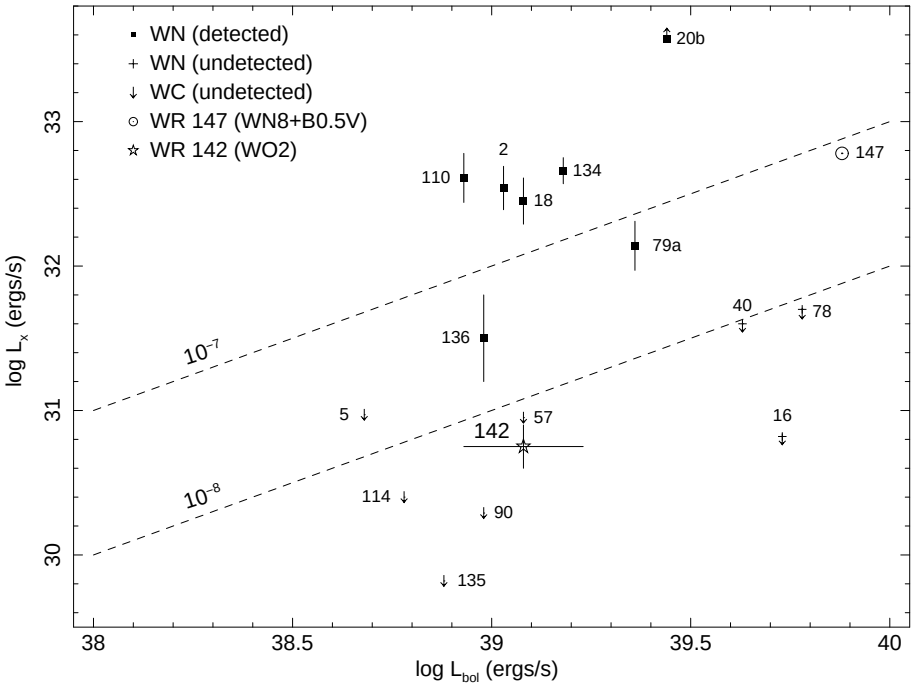

Fig. 5.— Adapted from Skinner et al. (2010b), with new points for WR 142 and WR 16. Note that WR 142 lies in the region of undetected WC stars. The dashed line marked 10^{-7} approximately follows the L_X versus L_{bol} relation for O- and early B-stars from *ROSAT* (Berghöfer et al. 1997), though a large scatter exists. The L_X value for WR 16 is based on a recent *XMM-Newton* observation (Observation Id 0602020301, obtained on 2009 Dec. 28). EPIC MOS images show a faint excess above background at the WR 16 position (13 net MOS2 counts in the 0.3 - 8 keV range, r = 15″ extraction circle = 68% encircled energy, 33 ksec of usable MOS2 exposure, 0.394 counts ksec^{-1}). Using PIMMS, the MOS2 count rate equates to an unabsorbed X-ray luminosity log L_X(0.3 - 8 keV) = 30.82 ergs s^{-1}, assuming d = 2.73 kpc and A_V = 1.85 (van der Hucht 2001), and an intrinsic 2T Raymond-Smith thermal plasma source spectrum with kT_1 = 0.6 keV and kT_2 = 3.5 keV. Because the X-ray detection of WR 16 is of low significance, its L_X value is plotted as an upper limit. L_{bol} for WR 16 is from Hamann et al. (2006).